inorganics

MDPI

Article

Trapping of an Heterometallic Unsaturated Hydride: Structure and Properties of the Ammonia Complex [MoMnCp(μ-H)(μ-PPh_2)$(CO)_5(NH_3)$]

M. Angeles Alvarez, Daniel García-Vivó *, Estefanía Huergo and Miguel A. Ruiz *

Departamento de Química Orgánica e Inorgánica/IUQOEM, Universidad de Oviedo, E-33071 Oviedo, Spain; maf@uniovi.es (M.A.A.); estefania.huergo@gmail.com (E.H.)

* Correspondence: garciavdaniel@uniovi.es (D.G.-V.), mara@uniovi.es (M.A.R.); Tel: +34-985102962 (D.G.-V.); +34-985102978 (M.A.R.)

Received: 15 October 2018; Accepted: 15 November 2018; Published: 24 November 2018

Abstract: Complexes displaying multiple bonds between different metal atoms have considerable synthetic potential because of the combination of the high electronic and coordinative unsaturation associated to multiple bonds with the intrinsic polarity of heterometallic bonds but their number is scarce and its chemistry has been relatively little explored. In a preliminary study, our attempted synthesis of the unsaturated hydrides [MoMCp(μ-H)(μ-PR_2)$(CO)_5$] from anions [MoMCp(μ-PR_2)$(CO)_5]^-$ and $(NH_4)PF_6$ yielded instead the ammonia complexes [MoMCp(μ-H)(μ-PR_2)$(CO)_5(NH_3)$] (M = Mn, R = Ph; M = Re, R = Cy). We have now examined the structure and behaviour of the MoMn complex (Mo–Mn = 3.087(3) Å) and found that it easily dissociates NH_3 (this requiring some 40 kJ/mol, according to DFT calculations), to yield the undetectable unsaturated hydride [MoMnCp(μ-H)(μ-PPh_2)$(CO)_5$] (computed Mo–Mn = 2.796 Å), the latter readily adding simple donors L such as CNR (R = Xyl, *p*-C_6H_4OMe) and $P(OMe)_3$, to give the corresponding electron-precise derivatives [MoMnCp(μ-H)(μ-PPh_2)$(CO)_5$(L)]. Thus the ammonia complex eventually behaves as a synthetic equivalent of the unsaturated hydride [MoMnCp(μ-H)(μ-PPh_2)$(CO)_5$]. The isocyanide derivatives retained the stereochemistry of the parent complex (Mo–Mn = 3.0770(4) Å when R = Xyl) but a carbonyl rearrangement takes place in the reaction with phosphite to leave the entering ligand *trans* to the PPh_2 group, a position more favoured on steric grounds.

Keywords: metal–metal multiple bonds; heterometallic complexes; hydride complexes; binuclear carbonyl complexes; density functional theory calculations

1. Introduction

The chemical behaviour of transition-metal complexes combining in the same molecule two or more close metal atoms of different elements (heterometallic complexes) is a living research area within modern Inorganic Chemistry. The combination of different electronic and coordination environments, as found in these molecules, produces cooperative and synergic effects eventually leading, when compared to complexes having just one type of metals (homometallic complexes), to higher reactivity and chemioselectivity, not only in stoichiometric processes of interest but also in catalytic ones [1–3]. It is not by accident that different relevant biological processes are only possible thanks to the action of different enzymes which in turn have heterometallic centres at their active sites, as it is the case of several nitrogenases, hydrogenases or dehydrogenases, which bear Fe–Co, V–Fe, Ni–Fe and related heterometallic active centres. Complexes displaying multiple bonds between distinct metal atoms are a class of heterometallic species of particular interest, since they combine the high electronic and

coordinative unsaturation inherent to multiple bonds with the polarity of heterometallic bonds, which should lead to increased reactivity, when compared to homometallic analogues [4–8]. Yet, the chemistry of these species has been relatively little explored so far, due to synthetic difficulties or easy degradation to mononuclear species during their reactions, particularly in the case of organometallic compounds. However, there are precedents indicating that organometallic substrates with heterometallic multiple bonds have a large potential for the stoichiometric and catalytic activation of small molecules. For instance, Chetcuti et al. studied complexes with Co=Ni bonds able to induce under mild conditions different isomerisation processes, as well as regiospecific C–C couplings and P–C bond cleavages [8,9], while Suzuki et al. studied unsaturated complexes with $Zr(\mu\text{-}H)_3Ir$ or $TaIr(H)_2$ centres able to activate C–H, N–H and O–H bonds [10,11]. The same group found that the unsaturated hydride $[Cp^*Ru(\mu\text{-}H)_4OsCp^*]$ undergoes addition reactions at a rate much higher than the rates measured for the corresponding homonuclear complexes having Ru–Ru or Os–Os bonds [12]. Therefore, the preparation of new organometallic complexes featuring heterometallic multiple bonds and stabilized towards degradation can be considered a relevant target in the current organometallic research. Recently, we reported the synthesis of the 32-electron complexes $[MoMCp(\mu\text{-}PR_2)(CO)_5]^-$ (**1**) (M = Mn, R = Ph; M = Re, R = Cy), which are the first examples of organometallic anions with group 6–7 metals having multiple M–M´ bonds [13]. Protonation of these anions with $(NH_4)PF_6$ did not yield the sought unsaturated hydride-bridged derivatives $[MoMCp(\mu\text{-}H)(\mu\text{-}PR_2)(CO)_5]$ but gave instead the corresponding ammonia complexes $[MoMCp(\mu\text{-}H)(\mu\text{-}PR_2)(CO)_5(NH_3)]$, this suggesting that the targeted unsaturated hydrides were very reactive species. Shortly after that, we found that the acetonitrile adduct $[MoReCp(\mu\text{-}H)(\mu\text{-}PCy_2)(CO)_5(NCMe)]$ underwent easy displacement of NCMe with different molecules such as phosphines, thiols or alkynes, thus effectively acting as a surrogate of the unsaturated hydride $[MoReCp(\mu\text{-}H)(\mu\text{-}PCy_2)(CO)_5]$ [14]. Given the similarity between the above Re complex and the ammonia complexes mentioned above, we wondered if the latter could also be used as synthetic equivalents of the elusive $[MoMCp(\mu\text{-}H)(\mu\text{-}PR_2)(CO)_5]$ hydrides. We have explored this idea on the Mo–Mn substrate and in this paper we report a more complete structural characterization of the ammonia complex $[MoMnCp(\mu\text{-}H)(\mu\text{-}PPh_2)(CO)_5(NH_3)]$ (**2**) and a computational study of the unsaturated hydride $[MoMnCp(\mu\text{-}H)(\mu\text{-}PPh_2)(CO)_5]$ (**H**) following from ammonia release in the former (Figure 1). We also report our results on the reactions of **2** with simple donors such as isocyanides and phosphites, which prove that this ammonia complex effectively acts as a synthetic equivalent of the elusive unsaturated hydride **H**. In this paper we have adopted a "half-electron" counting convention for complexes displaying bridging hydrides, so compound **H** is regarded as having a Mo=Mn bond, thus emphasizing its unsaturated nature (but see our DFT description of such a bond). Other authors, however, recommend the adoption of a "half-arrow" convention for all hydride-bridged complexes [15]. A discussion on both views on hydride-bridged complexes has been made recently [16].

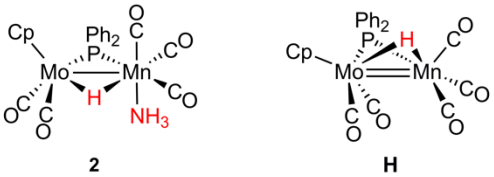

2 **H**

Figure 1. Structure of hydride complexes **2** and **H**.

2. Results and Discussion

2.1. Protonation of Anion **1**. *Structural Characterization of the Ammonia Complex* **2**

As noted in our preliminary study [13], the reaction of the unsaturated complex $Na[MoMnCp(\mu\text{-}PPh_2)(CO)_5]$ (**1-Na**) with $(NH_4)PF_6$ gives the ammonia complex **2** as the sole product (Scheme 1). Compound **2** is a poorly stable material easily decomposing upon manipulation, either in solution or in the solid state, to give the known hexacarbonyl complex

[MoMnCp(μ-H)(μ-PPh_2)$(CO)_6$] [17]. This suggests that ammonia coordination to manganese is quite weak in **2** and, accordingly, a separate experiment indicated that exposure of **2** to CO (1 atm) leads quantitatively to the above hexacarbonyl complex. Although we could not obtain compound **2** as an analytically pure product, we were able to grow, through low temperature crystallization, a few crystals suitable for an X-ray diffraction study. Even if the quality of the diffraction data was not high, the essential structural features of the molecule can be clearly defined (Figure 2 and Table 1).

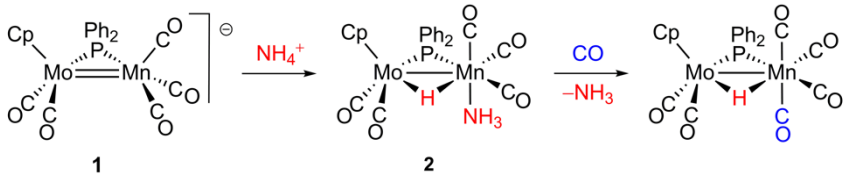

Scheme 1. Formation and decomposition of compound **2**.

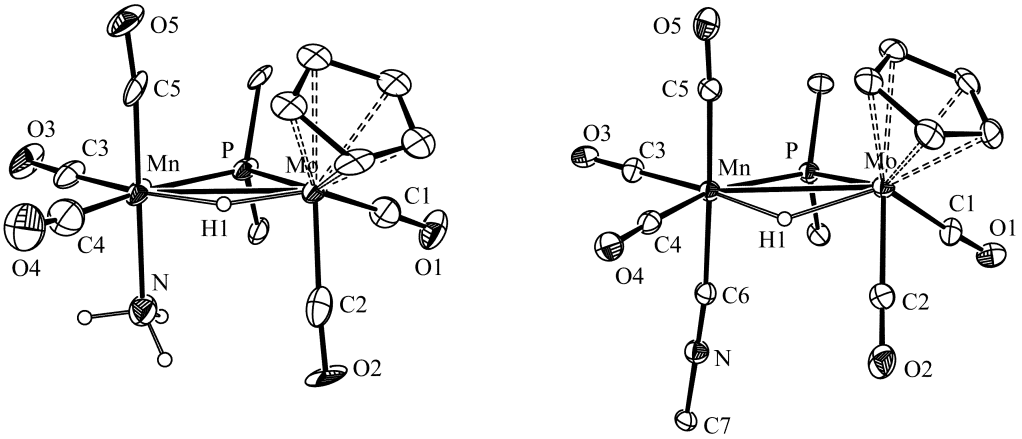

Figure 2. ORTEP drawing (30% probability) of compounds **2** (left) and **3a** (right), with aryl rings (except their C^1 atoms) and most H atoms omitted.

Table 1. Selected Bond distances (Å) and Angles (°) for Compounds **2** and **3a**.

Parameter	2	3a	Parameter	2	3a
Mo Mn	3.087(3)	3.0770(4)	P Mo C1	73.1(7)	78.7(1)
Mo P	2.446(4)	2.4405(6)	P Mo C2	105.3(6)	111.1(1)
Mn P	2.277(5)	2.2816(7)	P Mn C3	98.1(7)	101.1(1)
Mo H	1.56(1)	1.83(3)	P Mn C4	165.5(9)	161.5(1)
Mn H	1.82(1)	1.74(3)	P Mn C5	89.0(7)	91.7(1)
Mo C1	1.91(2)	1.973(3)	P Mn N1/C6	90.5(4)	88.0(1)
Mo C2	1.95(3)	1.962(3)	Mo P Mn	81.5(2)	81.25(2)
Mn C3	1.78(2)	1.793(3)	C6 N6 C7	-	179.6(3)
Mn C4	1.84(3)	1.819(3)	Mo Mn N/C6	92.9(5)	97.9(1)
Mn C5	1.80(2)	1.827(3)	-	-	-
Mn N1/C6	2.10(2)	1.919(3)	-	-	-

The structure of **2** in the crystal is very similar to that of its rhenium analogue [13] and is made of $MoCp(CO)_2$ and $Mn(CO)_3(NH_3)$ fragments bridged by PPh_2 and H ligands. The carbonyls around the manganese atom are in a facial arrangement and the ammonia ligand is positioned *cis* to the bridging ligands and *anti* to the Cp ring of the molybdenum fragment. Overall, compound **2** is a 34-electron complex for which a metal–metal single bond has to be formulated according to the 18-electron rule, which is consistent with the intermetallic separation of 3.087(3) Å, almost identical to the separation of 3.088(1) Å determined in the hexacarbonyl complex [MoMnCp(μ-H)(μ-PPh_2)$(CO)_6$] [18]. As for the ammonia coordination, we note that the Mn–N length of 2.10(2) Å in **2** exactly matches the reference

single-bond length of 2.10 Å for these atoms [19] and therefore is not particularly elongated. This length also is essentially identical to the values measured in the cation $[Mn(CO)_3(NH_3)_3]^+$, which appears to be the only other Mn(I) ammonia complex structurally characterized to date [20]. In contrast, ammonia ligands bound to paramagnetic Mn(II) centres display larger Mn N separations of ca. 2.24 Å [21].

Spectroscopic data in solution for **2** (Table 2 and Section 3) are fully consistent with the structure found in the crystal. Its IR spectrum in solution displays five C–O stretching bands, with the most energetic one (mainly corresponding to the symmetrical stretch of the $Mn(CO)_3$ fragment) being of high intensity, which is indicative of a facial arrangement of the carbonyls around the Mn atom [22]. Its ^{31}P NMR resonance appears at 161.4 ppm, some 30 ppm more deshielded than the corresponding resonance in the parent unsaturated anion **1** but in any case consistent with the presence of a phosphanyl ligand bridging a metal–metal bond [23]. The ammonia ligand gives rise to a relatively shielded ^1H NMR resonance at −1.39 ppm, while the bridging hydride gives rise to a strongly shielded and P-coupled resonance, as expected (δ −12.52 ppm, J_{HP} = 38 Hz). These data are comparable to those measured for the analogous Re complex (−0.06 ppm and −10.56 ppm, J_{HP} = 20 Hz respectively) [13], with the differences in chemical shifts and P–H couplings being the expected ones when replacing a first-row atom (Mn) with a third-row one (Re) [24].

Table 2. Selected IR [1], and $^{31}P\{^1H\}$ Data [2] for New Compounds.

Compound	ν(CO)	δ(P)
Na[MoMnCp(μ-PPh_2)$(CO)_5$] (**1-Na**) [3]	1968 (s), 1881 (vs) 1864 (s, sh), 1804 (w)	131.3
[MoMnCp(μ-H)(μ-PPh_2)$(CO)_5(NH_3)$] (**2**)	2001 (s), 1944 (vs), 1915 (s), 1893 (m), 1866 (m) [4]	161.4 [5]
[MoMnCp(μ-H)(μ-PPh_2)$(CO)_5$(CNXyl)] (**3a**)	2009 (s), 1951 (vs) 1931 (m, sh), 1871 (w)	160.9 [6]
[MoMnCp(μ-H)(μ-PPh_2)$(CO)_5${CN(*p*-C_6H_4OMe)}] (**3b**)	2010 (s), 1949 (vs) 1933 (s, sh), 1870 (m)	160.9
[MoMnCp(μ-H)(μ-PPh_2)$(CO)_5${P$(OMe)_3$}] (**4**)	2030 (w), 1951 (vs) 1925 (m, sh), 1869 (m)	191.81 63.9 (μ-P)

[1] Recorded in dichloromethane solution, with C–O stretching bands [ν(CO)] in cm^{-1}. [2] Recorded in benzene-d_6 solution at 121.49 MHz and 293 K, with chemical shifts (δ) in ppm. [3] Data taken from reference 13, recorded in tetrahydrofuran. [4] In tetrahydrofuran solution; ν(NH): 3381, 3365, 3288 cm^{-1} in Nujol mull. [5] In toluene-d_8, at 213 K. [6] In CD_2Cl_2 solution.

2.2. Mechanism of Formation of **2**. *DFT Calculations on the Putative Hydride Intermediate* **H**

The reaction of anion **1** with the NH_4^+ cation is expected to be initiated with a proton transfer from the latter to the dimetal centre of the former, to give the unsaturated hydride **H** (Scheme 2). This is likely to involve the π component of the Mo=Mn bond of **1**, which is the HOMO−2 of the molecule, as the donor orbital. Because of the spatial distribution of the latter orbital, the hydrogen atom is expected to be positioned so as to define a puckered MoPMnH central ring, as experimentally observed in the addition of the $[Au\{P(p\text{-}C_6H_4Me)_3\}]^+$ cation (isolobal with H^+) to anion **1** [13]. In a second step, the ammonia released in the proton transfer event would coordinate to the unsaturated hydride **H**, to give the electron-precise product **2** eventually isolated. This should take place at the coordinatively unsaturated manganese atom and in a position *anti* with respect to the Mo-bound Cp ligand (Scheme 2), a position more favoured on steric grounds, thus explaining the relative arrangement of these ligands found in the final product.

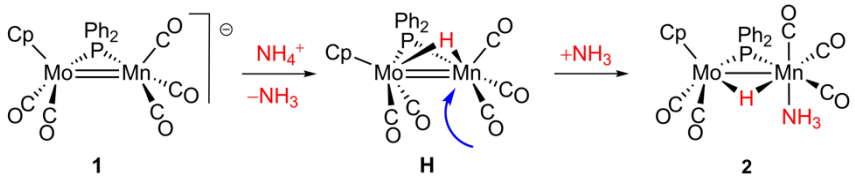

Scheme 2. Mechanism of formation of compound **2**.

To further support the above hypothesis, we have carried out density functional theory (DFT) calculations on intermediate **H** and we have found that the presumed structure is a minimum in the corresponding potential energy surface (Figure 3, see Section 3 and the Supplementary Materials for further details). The structure of hydride **H** can be related to that of the gold cluster [AuMoMnCp(μ-PPh_2)$(CO)_5${P(*p*-$C_6H_4Me)_3$}] [13] and indeed it displays a strongly puckered MoPMnH central ring (P–Mo–Mn–H = 108.5°) and a short Mn–Mo distance of 2.796 Å, as expected for an unsaturated species (cf. 2.705(1) Å in the above gold cluster), well below the distance of 3.088(1) Å measured in the saturated complex [MoMnCp(μ-H)(μ-PPh_2)$(CO)_6$] [18]. We note that B3LYP-DFT computed distances involving metal atoms usually are overestimated (by ca. 0.05 Å) when compared to distances measured by X-ray diffraction [25,26].

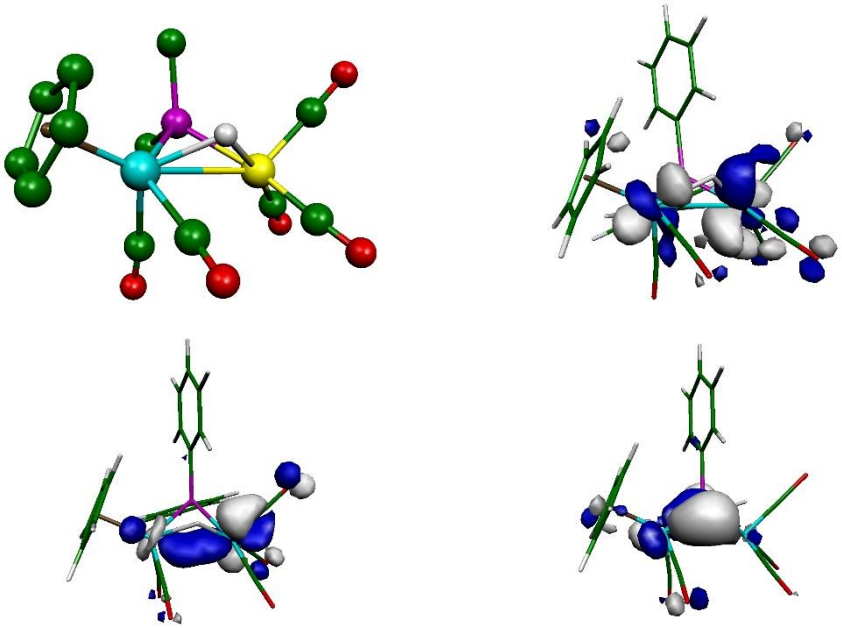

Figure 3. B3LYP-DFT computed structure of the unsaturated hydride **H** (upper left, with Ph rings and most H atoms omitted) along with the corresponding LUMO (upper right, −2.25 eV), HOMO−5 (lower left, −6.82 eV) and HOMO−12 orbitals (−8.74 eV).

Although there is considerable orbital mixing, the double bond formulated for hydride **H** still can be visualized as made up from the expected σ component (HOMO−5) and a closed tricentric MoHMn interaction (HOMO−12, here mixed with M–P bonding) which is derived from interaction of the π (Mo–Mn) bonding orbital in the parent anion **1** with the *s* orbital of hydrogen. Thus, rather than a conventional double bond made up of σ and π components, the double Mo=Mn bond in **H** is made up of a bicentric σ Mo–Mn interaction and a closed tricentric MoHMn interaction, in a way comparable to that recently described by us for the homometallic hydride [W_2Cp_2(μ-H)(μ-PPh_2)$(NO)_2$] [27]. Similar tricentric MHM interactions are also present in the 30-electron complexes [M_2Cp(μ-H)(μ-PCy_2)$(CO)_2$] complexes (M = Mo, W) [28–30]. Analysis of the electron density at the intermetallic region, under the Atoms in Molecules (AIM) framework [31], also supports the presence of substantial multiplicity in the intermetallic bond of hydride **H**. Thus, although a bond critical point was not strictly located, the

minimum electron density at the intermetallic axis was found to be 0.284 eÅ^{-3}, a figure substantially higher than the corresponding value computed by us at the same level for the electron-precise anion [MoMnCp(μ-PPh_2)$(CO)_6$]$^-$ (0.204 eÅ^{-3}) and only a bit below the value of 0.319 eÅ^{-3} computed at the intermetallic bond critical point in the unsaturated anion **1** [13]. In agreement with the above considerations, the intermetallic Mayer bond index in hydride **H** (0.43) is found to be lower than the one in the unsaturated anion **1** (0.56) but larger than the one computed for [MoMnCp(μ-PPh_2)$(CO)_6$]$^-$ (0.37) at the same level.

Finally, as concerning the reactivity of hydride **H**, we note that its LUMO orbital has π*(Mo–Mn) character (Figure 3) and its spatial distribution is suited for incorporation of a generic donor at the pocket region of the puckered MPMnH ring of the molecule, so the latter should take place in a position *anti* with respect to the Cp ring and should reduce the strength of the intermetallic bond, as observed in the formation of the ammonia complex **2**. In the case of ammonia, however, this addition process is only moderately favoured, since the computed Gibbs free energy for the gas-phase reaction **H** + NH_3 → **2** is only −41 kJ/mol at 295 K. From this it can be concluded that the reverse process, that is, ammonia dissociation from **2**, should be easily affordable at room temperature, in agreement with the low stability of **2** observed experimentally. Moreover, such an easy dissociation should enable **2** to behave as a synthetic equivalent of the unsaturated hydride **H**, when faced to molecules having donor properties better than those of ammonia, as confirmed through the experiments discussed in the next sections.

2.3. Reaction of **2** with Isocyanides

Compound **2** reacts readily with aryl isocyanides at room temperature or below to give the corresponding derivatives [MoMnCp(μ-H)(μ-PPh_2)$(CO)_5$(CNR)] in high yield [R = Xyl (**3a**), *p*-C_6H_4OMe (**3b**)], these following from displacement of the ammonia molecule by the isocyanide ligand, with retention of stereochemistry (Scheme 3). In agreement with this, the overall process **2** + CNXyl → **3a** + NH_3 was computed to be strongly favoured in the gas phase (ΔG = −370 kJ/mol at 295 K). A similar complex was prepared previously by Mays et al. upon photolysis of [MoMnCp(μ-H)(μ-PPh_2)$(CO)_6$] in the presence of $CNCH_2Ph$. The yield of this product, however, was much lower (23%) because of the competitive formation of double-substitution products [17]. This provides a clear example of the synthetic advantages of using precursors reactive enough at room temperature or below, when compared to the use of precursors being only reactive upon thermal or photochemical activation.

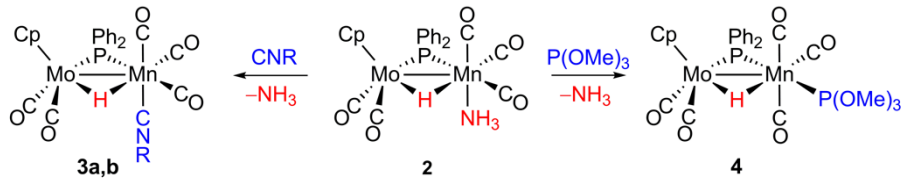

Scheme 3. Reactions of compound **2** with isocyanides and $P(OMe)_3$ (R = Xyl, 4-*p*C_6H_4OMe).

The structure of compound **3a** has been confirmed through an X-ray diffraction study. The molecule can be derived from that of the ammonia precursor **2** by just replacing the NH_3 ligand with a CNXyl molecule, which is coordinated to the Mn atom in a conventional linear fashion (Mn–C6 = 1.919(3) Å, C6–N–C7 = 179.6(3)°) and positioned *anti* with respect to the Cp ligand (Figure 2 and Table 1). The precision of the geometrical parameters here is much higher than was in **2**, so the location of the hydride ligand now is more reliable, it being found closer to the lighter Mn atom as expected (1.74(3) vs. 1.83(3) Å). These values compare well with those determined for the phosphinocyclopentadienyl-bridged complex [MoMn(μ-η^5:κ^1-$C_5H_4PPh_2$)(μ-H)(μ-PPh_2)$(CO)_5$] (1.76(3) and 1.83(3) Å) [32]. The same comment applies to the bridging PPh_2 ligand, with the difference in the M–P distances (2.2816(7) vs. 2.4405(6) Å) now almost matching the 0.15 Å difference in the covalent

radii of Mo and Mn [19]. We also note that the central MoPMnH ring (P–Mo–Mn–H = 156°) in **3a** is a bit more puckered than was in **2** (experimental 175°, computed 165°, see the Supplementary Materials). This likely has a steric origin, since such as distortion displaces the bulky Xyl group away from the crowded dimetal centre (Mo–Mn–C6 ca. 98°). The puckering of the central ring of **3a** also enables a closer approach of the metal atoms to each other, which now display a slightly shorter intermetallic separation (3.0770(4) vs. 3.087(3) Å in **2**).

Spectroscopic data in solution for compounds **3a** and **3b** are similar to each other and consistent with the structure found for **3a** in the solid state. Their IR spectra display a high-frequency C–N stretch above 2100 cm^{-1}, as expected for linear isocyanides, and four C–O stretches in the range 2010–1870 cm^{-1}. The high intensity of the most energetic C–O stretch in each case (at ca. 2010 cm^{-1}) again denotes the facial arrangement of the three carbonyls bound to manganese, as found for **2**. The P–C couplings observed for the carbonyl resonances in the ^{13}C NMR spectrum of **3a** also are consistent with its solid-state structure, with the Mo-bound carbonyl *cis* to the P atom displaying a P–C coupling larger than the one positioned *trans* to it (J_{CP} = 24 and ca. 0 Hz, respectively), while the reverse holds for carbonyls bound to the octahedral manganese centre, with the inequivalent carbonyls *cis* to P displaying a negligible coupling, while the one positioned *trans* to the P ligand (δ_C 213.9 ppm) displays a measurable coupling of 17 Hz. We recall here that a general trend established for $^2J_{XY}$ in complexes of the type [MCpXYL$_2$] is that $|J_{cis}| > |J_{trans}|$ [24,33].

2.4. Reaction of **2** with P(OMe)$_3$

Compound **2** reacts rapidly with a slight excess P(OMe)$_3$ at room temperature to give the corresponding phosphite complex [MoMnCp(μ-H)(μ-PPh$_2$)(CO)$_5${P(OMe)$_3$}] (**4**) as a sole product, which is isolated in 83% yield after conventional workup (Scheme 3). This complex was previously prepared by Mays et al. in moderate yield (23%) upon photolysis of [MoMnCp(μ-H)(μ-PPh$_2$)(CO)$_6$] in the presence of P(OMe)$_3$ [17]. Although the ^{31}P NMR and IR data reported for this product are identical to those recorded for **4** by us (Table 2), the structure then proposed actually is not consistent with the IR spectrum of this product. Indeed, this complex was originally proposed to have the P(OMe)$_3$ ligand positioned *cis* to the PPh$_2$ bridge (as found for compounds **2** and **3**). However, the IR spectrum of **4** is very different from those of **2** and **3** (Table 2 and Figure S2) in that the most energetic C–O stretching band (mainly arising from the symmetrical vibration of the Mn(CO)$_3$ fragment) appears at a somewhat higher frequency (2030 cm^{-1} instead of ca. 2010 cm^{-1}) and with *weak* intensity, the latter being a definitive indication of a meridional arrangement of the three CO ligands surrounding the manganese atom [22]. Having established this carbonyl arrangement, then the positioning of the P(OMe)$_3$ ligand *trans* to the PPh$_2$ group is deduced from the fact that the hydride resonance of **4** (δ_H −13.80 ppm) displays identical two-bond P–H couplings of 30 Hz to both P-donor ligands, which is indicative of a positioning of the hydride ligand *cis* to both P atoms.

The reaction of **2** with P(OMe)$_3$, however, is likely initiated the same way as the one with isocyanides, to give an intermediate species **F** (undetected) analogous to complexes **2** and **3**, that is, with the P(OMe)$_3$ ligand positioned *cis* to the PPh$_2$ bridge and *anti* with respect to the Cp ligand (Scheme 4). This intermediate would then rapidly rearrange into the final isomer **4**, which is more favoured on steric grounds, as the P(OMe)$_3$ ligand is thus placed away from the bulky PPh$_2$ group. Under this view, we would expect that the related PPh$_3$ complex [MoMnCp(μ-H)(μ-PPh$_2$)(CO)$_5$(PPh$_3$)], reported by Mays et al. using their photochemical route, would display a structure comparable to that of **4**, with a transoid positioning of the PPh$_2$ and PPh$_3$ ligands and a meridional arrangement of carbonyls around the manganese atom. Interestingly, the IR spectrum reported for this product includes a symmetrical C–O stretch of *medium* intensity at a frequency higher than the one for the related CNCH$_2$Ph complex (2027 (m) vs. 2015 (s) cm^{-1}, in petroleum ether). This might be consistent with a structure for the PPh$_3$ complex analogous to that of **4** and not to those of **2** and **3**, as originally assumed [17].

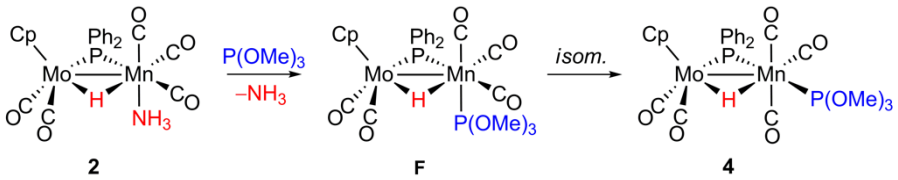

Scheme 4. Proposed reaction pathway in the formation of compound **4**.

3. Materials and Methods

3.1. General Procedures and Starting Materials

All manipulations and reactions were carried out under an argon (99.995%) atmosphere using standard Schlenk techniques. Solvents were purified according to literature procedures and distilled prior to use [34]. Tetrahydrofuran solutions of compound Na[MoMnCp(μ-PPh_2)$(CO)_5$] (**1-Na**) were prepared in situ as described previously [13] and used without further purification. All other reagents were obtained from the usual commercial suppliers and used as received, unless otherwise stated. Petroleum ether refers to that fraction distilling in the range 338–343 K. Chromatographic separations were carried out using jacketed columns refrigerated by tap water (ca. 288 K). Aluminium oxide for chromatography (activity I, 70–290 mesh) was degassed under vacuum prior to use and then was mixed under argon with the appropriate amount of water to reach activity IV. IR (Perkin Elmer, Waltham, MA, USA) stretching frequencies of CO ligands were measured in solution or in Nujol mulls (using CaF_2 windows in both cases) and are referred to as ν(CO)(solvent) or ν(CO)(Nujol), respectively. Nuclear magnetic resonance (NMR) (Bruker, Hamburg, Germany) spectra were routinely recorded at 300.13 (^{1}H), 121.49 (^{31}P{^{1}H}) or 100.63 MHz (^{13}C{^{1}H}), at 295 K unless otherwise stated. Chemical shifts (δ) are given in ppm, relative to internal tetramethylsilane (^{1}H, ^{13}C) or external 85% aqueous H_3PO_4 (^{31}P). Coupling constants (*J*) are given in Hertz.

3.2. Preparation of [MoMnCp(μ-H)(μ-PPh_2)$(CO)_5(NH_3)$] (**2**)

A solution containing ca. 0.030 mmol of compound **1-Na** in tetrahydrofuran (8 mL) was stirred with an excess $(NH_4)PF_6$ (ca. 0.040 g, 0.245 mmol) for 3 min to give a pale yellow solution. The solvent was then removed under vacuum and the residue was extracted with petroleum ether and filtered using a canula. Removal of the solvent under vacuum gave a yellow residue containing essentially pure compound **2**, amenable to spectroscopic characterization and ready for further use. Unfortunately, all our attempts to isolate this complex as a pure solid material were unsuccessful due to its progressive decomposition upon manipulation, this preventing from obtaining a satisfactory elemental analysis for this compound. However, a few X-ray quality crystals could be obtained by the slow diffusion of a layer of petroleum ether into a concentrated toluene solution of the crude product at 253 K. ν(CO)(petroleum ether): 2009 (s), 1951 (vs), 1926 (s), 1907 (s), 1873 (m) cm^{-1}. ν(NH)(Nujol): 3381, 3365, 3288 cm^{-1}. ν(CO)(Nujol): 2000 (s), 1940 (vs), 1931 (sh, s), 1903 (s), 1871 (m) cm^{-1}. ^{1}H NMR (400.13 MHz, tol-d_8, 213 K): δ 8.10-6.74 (m, 10H, Ph), 4.39 (s, 5H, Cp), −1.39 (s, 3H, NH_3), −12.52 (d, J_{HP} = 38, 1H, μ-H) (see Figure S4). ^{13}C{^{1}H} NMR (tol-d_8, 213 K): δ 242.2 (d, J_{CP} = 25, MoCO), 239.2 (s, MoCO), 224.0 (d, J_{CP} = 15, MnCO), 223.8 (d, J_{CP} = 15, MnCO), 219.8 (d, J_{CP} = 16, MnCO), 141.3 [d, J_{CP} = 36, C^1(Ph)], 140.3 [d, J_{CP} = 30, C^1(Ph)], 135.0 [d, J_{CP} = 8, 2C^2(Ph)], 132.7 [d, J_{CP} = 9, 2C^3(Ph)], 132.0, 131.9 [2s, C^4(Ph)], 91.7 (s, Cp).

3.3. Preparation of [MoMnCp(μ-H)(μ-PPh_2)$(CO)_5$(CNXyl)] (**3a**)

A solution of CNXyl (120 μL of a 0.05 M solution in petroleum ether, 0.060 mmol; Xyl = 2,6-$C_6H_3Me_2$) was added to a solution of compound **2** (ca. 0.025 g, 0.045 mmol) in tetrahydrofuran (8 mL) at 273 K and the mixture was stirred at this temperature for 30 min to give an orange solution. The solvent was then removed under vacuum, the residue extracted with dichloromethane/petroleum ether (1:7) and the extracts chromatographed on alumina. Elution with dichloromethane/petroleum

ether (1:5) gave an orange fraction yielding, after removal of solvents, compound **3a** as an orange microcrystalline solid (0.020 g, 65%). The crystals used in the X-ray study were grown by the slow diffusion of a layer of petroleum ether into a concentrated dichloromethane solution of the complex at 253 K. Anal. Calcd. for $C_{31}H_{25}MnMoNO_5P$: C, 55.29; H, 3.74; N, 2.08. Found: C, 54.93; H, 3.35; N, 2.21. ν(CO)(CH_2Cl_2): 2138 (w, C–N), 2009 (vs), 1951 (vs), 1931 (sh, m), 1871 (w), see Figure S2. ^{1}H NMR (CD_2Cl_2): δ 8.14-6.76 (m, 13H, Ph and C_6H_3), 5.05 (s, 5H, Cp), 1.86 (s, 6H, Me), −13.62 (d, J_{HP} = 36, 1H, μ-H). ^{13}C{^{1}H} NMR (CD_2Cl_2, 213 K): δ 243.4 (d, J_{CP} = 24, MoCO), 236.7 (s, MoCO), 221.1 (s, MnCO), 220.5 (s, MnCO), 213.9 (d, J_{CP} = 17, MnCO), 170.5 (s, CN), 140.1 [d, J_{CP} = 30, C^1(Ph)], 139.7 [d, J_{CP} = 33, C^1(Ph)], 134.5–125.9 (m, Ph and C_6H_3), 91.0 (s, Cp), 17.1 (s, Me).

3.4. Preparation of [MoMnCp(μ-H)(μ-PPh$_2$)(CO)$_5${CN(p-C$_6$H$_4$OMe)}] (**3b**)

Neat CN(*p*-C_6H_4OMe) (0.030 g, 0.218 mmol) was added to a solution of compound **2** (ca. 0.025 g, 0.045 mmol) in tetrahydrofuran (8 mL) and the mixture was stirred at room temperature for 1 min to give an orange solution. The solvent was then removed under vacuum, the residue extracted with dichloromethane/petroleum ether (1:7) and the extracts chromatographed on alumina. Elution with the same solvent mixture gave an orange fraction yielding, after removal of solvents, compound **3b** as an orange microcrystalline solid (0.022 g, 72%). Anal. Calcd. for $C_{30}H_{23}MnMoNO_6P$: C, 53.35; H, 3.43; N, 2.07. Found: C, 52.97; H, 3.20; N, 2.35. ν(CO)(CH_2Cl_2): 2147 (w, C–N), 2010(s), 1949 (vs), 1933 (s, sh), 1870 (m). ^{1}H NMR (C_6D_6): δ 8.25–6.04 (m, 14H, Ph and C_6H_4), 4.61 (s, 5H, Cp), 3.01 (s, 3H, OMe), −13.31 (d, J_{HP} = 34, 1H, μ-H).

3.5. Preparation of [MoMnCp(μ-H)(μ-PPh$_2$)(CO)$_5${P(OMe)$_3$}] (**4**)

Neat $P(OMe)_3$ (14 μL, 0.064 mmol) was added to a solution of compound **2** (ca. 0.025 g, 0.045 mmol) in tetrahydrofuran (8 mL) and the mixture was stirred at room temperature for 10 min to give an orange solution. The solvent was then removed under vacuum, the residue extracted with petroleum ether and the extracts chromatographed on alumina. Elution with dichloromethane/petroleum ether (1:5) gave an orange fraction yielding, after removal of solvents, compound **4** as an orange microcrystalline solid (0.025 g, 83%). Anal. Calcd. for $C_{25}H_{25}MnMoNO_8P_2$: C, 45.07; H, 3.78. Found: C, 44.75; H, 3.47. ν(CO)(petroleum ether): 2033 (w), 1959 (vs), 1950 (sh, m), 1934 (m), 1883 (w). ^{1}H NMR (C_6D_6): δ 8.22–6.76 (m, 10H, Ph), 4.68 (s, 5H, Cp), 3.48 (d, J_{HP} = 11, 9H, OMe), −13.80 (t, J_{HP} = 30, 1H, μ-H).

3.6. X-ray Structure Determination of Compounds **2** *and* **3a**

Data collection for these compounds was performed at ca. 155 K on an Oxford Diffraction Xcalibur Nova single crystal diffractometer (Agilent, Santa Clara, CA, USA), using Cu Kα radiation. Images were collected at a 62 mm fixed crystal-detector distance using the oscillation method, with 1.2° (**2**) or 1.1° (**3a**) oscillation and variable exposure time per image. Data collection strategy was calculated with the program CrysAlis Pro CCD [35] and data reduction and cell refinement was performed with the program CrysAlis Pro RED [35]. An empirical absorption correction was applied using the SCALE3 ABSPACK algorithm as implemented in the program CrysAlis Pro RED. Using the program suite WINGX [36], the structures were solved by Patterson interpretation and phase expansion using *SHELXL*2016 [37,38] and refined with full-matrix least squares on F^2 using *SHELXL*2016. In general, the positional parameters and anisotropic temperature factors for all non-H atoms were refined anisotropically and hydrogen atoms were geometrically placed and refined using a riding model. In the case of **3a**, the hydride atom H(1) was located in the Fourier maps and refined isotropically. In the case of compound **2**, the quality of the diffraction data was poor and a fully satisfactory model could not be achieved, although the main structural features of the complex could be firmly established. In that case, the complex crystallized with a disordered toluene molecule which could be modelled over two positions with 0.7/0.3 occupancies, along with some restraints and SIMU and DELU instructions. For the molecule of the complex, a fully anisotropic model was attempted but, due to the poor quality of the diffraction data, not all the positional parameters and anisotropic

temperature factors for non-H atoms could be refined anisotropically. Two carbon atoms of the cyclopentadienyl ligand had to be refined anisotropically in combination with the instructions DELU and SIMU and two carbon atoms of carbonyl ligands were refined isotropically to prevent their temperature factors from becoming non-positive definite. All hydrogen atoms were geometrically placed and refined using a riding model, except for the hydride ligand and the ammonia hydrogen atoms, which were located in the Fourier maps: the hydride atom was refined isotropically and the ammonia H atoms were refined riding on their parent atom with some restraints on the N–H distances. After convergence, some large residual electron density peaks remained in the difference maps and the overall agreement factors were very poor (R_1 ca. 0.24) (Table 3). CCDC-1871692 and 1871693 contain the full crystallographic data for compounds **2** and **3a**. These data can be obtained free of charge via http://www.ccdc.cam.ac.uk/conts/retrieving.html (or from the CCDC, 12 Union Road, Cambridge CB2 1EZ, UK; Fax: +44-1223-336033; E-mail: deposit@ccdc.cam.ac.uk).

Table 3. Crystal Data for New Compounds.

Parameter	**2**·C_7H_8	**3a**
mol formula	$C_{29}H_{27}MnMoNO_5P$	$C_{31}H_{25}MnMoNO_5P$
mol wt	651.37	673.37
cryst syst	monoclinic	triclinic
space group	$P2_1/c$	$P\,1$
radiation (λ, Å)	1.54184	1.54184
a, Å	19.0906(14)	10.9412(6)
b, Å	8.5500(4)	11.1757(6)
c, Å	17.2528(11)	11.9618(6)
α, deg	90	84.979(4)
β, deg	100.240(6)	78.905(5)
γ, deg	90	84.550(4)
V, Å^3	2771.2(3)	1425.22(13)
Z	4	2
calcd density, g·cm^{-3}	1.561	1.569
absorp coeff, mm^{-1}	8.285	8.080
temperature, K	154(5)	156(5)
θ range (deg)	4.71–69.41	3.76–69.69
index ranges (*h*; *k*; *l*)	−22, 21; −10, 8; −20, 15	−12, 13; −13, 13; −14, 12
no. of reflns collected	12,356	12,082
no. of indep reflns (R_{int})	5094(0.0912)	5243(0.0320)
reflns with $I > 2\sigma(I)$	4275	4743
R indexes [data with $I > 2\sigma(I)$] [a]	R_1 = 0.2410, wR_2 = 0.5368 [b]	R_1 = 0.0276, wR_2 = 0.0721 [c]
R indexes (all data) [a]	R_1 = 0.2510, wR_2 = 0.5492 [b]	R_1 = 0.0316, wR_2 = 0.0752 [c]
GOF	2.390	1.058
no. of restraints/params	24/305	0/367
Δρ(max./min.), eÅ^{-3}	10.949/−3.325	0.480/−0.662
CCDC deposition no	1871692	1871693

[a] $R = \sum||F_o| - |F_c||/\sum|F_o|$. $wR = [\sum w(|F_o|^2 - |F_c|^2)^2/\sum w|F_o|^2]^{1/2}$. $w = 1/[\sigma^2(F_o^2) + (aP)^2 + bP]$ where $P = (F_o^2 + 2F_c^2)/3$. [b] $a = 0.2000$, $b = 0.0000$. [c] $a = 0.0423$, $b = 0.0966$.

3.7. Computational Details

All DFT calculations were carried out using the GAUSSIAN03 package [39], in which the hybrid method B3LYP was used with the Becke three-parameter exchange functional [40] and the Lee-Yang-Parr correlation functional [41]. Inclusion of the empirical dispersion correction developed by Grimme (B3LYP-D) [42], gave essentially the same results (see the Supplementary Materials). A pruned numerical integration grid (99,590) was used for all the calculations via the keyword Int=Ultrafine. Effective core potentials and their associated double-ζ, LANL2DZ basis set were used for Mo and Mn atoms [43]. The light elements (P, N, O, C and H) were described with the 6-31G* basis [44–46]. Geometry optimizations were performed under no symmetry restrictions, using initial coordinates

derived from the X-ray data of closely related compounds and frequency analyses were performed for all the stationary points to ensure that a minimum structure with no imaginary frequencies was achieved. Molecular orbitals and vibrational modes were visualized using the MOLEKEL program [47] and the topological analysis of the electron density was carried out with the MultiWFN program [48].

4. Conclusions

According to DFT calculations, the ammonia ligand in the title complex is weakly coordinated to the manganese atom, so it can dissociate easily at room temperature. The latter event renders the unsaturated hydride complex [MoMnCp(μ-H)(μ-PPh_2)$(CO)_5$] (**H**), with a geometric and electronic structure that enables it to add any donor molecule at the site formerly occupied by the ammonia ligand. As a result of all of this, the ammonia complex effectively behaves as a synthetic equivalent of the unsaturated hydride **H** and therefore can be viewed as a sort of trapped form of **H**. From the results of reactions analysed so far, it can be concluded that reactions of the ammonia complex with simple donor ligands likely will take place initially with retention of stereochemistry but further migration of the entering molecule to a position *trans* to the PPh_2 bridging ligand is expected for bulky donor molecules.

Supplementary Materials: The following are available online at http://www.mdpi.com/2304-6740/6/4/125/s1: A PDF file containing: Figure S1: Structure of compound **H**. Table S1: Geometry of **H**. Table S2: Selected molecular orbitals for **H**. Figure S2: IR spectra for compounds **3a** and **4**. Figure S3: IR spectrum of compound **2**. Figure S4: 1H NMR spectrum of compound **2**. An XYZ file containing the Cartesian coordinates of all computed species, a CIF file containing full crystallographic data for compounds **2** and **3a**, and the corresponding checkcif file.

Author Contributions: D.G.-V. and M.A.R. designed the experiments and wrote the paper; E.H. performed the experimental work; M.A.A. carried out the crystal structure determinations; D.G.-V. performed the theoretical computations.

Funding: This research was funded by the MINECO of Spain and FEDER (Project CTQ2015-63726-P and a grant to E.H.) and the Consejería de Educación of Asturias (Project GRUPIN14-011).

Acknowledgments: We also thank the X-Ray unit of the Universidad de Oviedo for the acquisition of diffraction data and the SCBI of the Universidad de Málaga, Spain, for access to computing facilities.

Conflicts of Interest: The authors declare no conflict of interest.

References

1. Knorr, M.; Jourdain, I. Activation of alkynes by diphosphine- and μ-phosphido-spanned heterobimetallic complexes. *Coord. Chem. Rev.* **2017**, *350*, 217–247. [CrossRef]
2. Mankad, N.P. Selectivity Effects in Bimetallic Catalysis. *Chem. Eur. J.* **2016**, *22*, 5822–5829. [CrossRef] [PubMed]
3. Buchwalter, P.; Rosé, J.; Braunstein, P. Multimetallic Catalysis Based on Heterometallic Complexes and Clusters. *Chem. Rev.* **2015**, *115*, 28–126. [CrossRef] [PubMed]
4. Eisenhart, R.J.; Clouston, L.J.; Lu, C.C. Configuring Bonds between First-Row Transition Metals. *Acc. Chem. Res.* **2015**, *48*, 2885–2894. [CrossRef] [PubMed]
5. Krogman, J.P.; Thomas, C.M. Metal-metal multiple bonding in C_3-symmetric bimetallic complexes of the first row transition metals. *Chem. Commun.* **2014**, *540*, 5115–5127. [CrossRef] [PubMed]
6. Thomas, C.M. Metal-Metal Multiple Bonds in Early/Late Heterobimetallic Complexes: Applications Toward Small Molecule Activation and Catalysis. *Comments Inorg. Chem.* **2011**, *32*, 14–38. [CrossRef]
7. Ritleng, V.; Chetcuti, M.J. Hydrocarbyl Ligand Transformations on Heterobimetallic Complexes. *Chem. Rev.* **2007**, *107*, 797–858. [CrossRef] [PubMed]
8. Collman, J.P.; Boulatov, R. Heterodinuclear Transition-Metal Complexes with Multiple Metal–Metal Bonds. *Angew. Chem. Int. Ed.* **2002**, *41*, 3948–3961. [CrossRef]
9. Clapham, S.; Braunstein, P.; Boag, N.M.; Welter, R.; Chetcuti, M.J. Carbon−Phosphorus Bond Cleavage in Allyldiphenylphosphine by a Heterobimetallic Ni=Mo Complex and Formation of an Electronically Unsaturated $NiMo_2$ μ-Diphenylphosphido Cluster. *Organometallics* **2008**, *27*, 1758–1764. [CrossRef]

10. Oishi, M.; Oshima, M.; Suzuki, H. A Study on Zr–Ir Multiple Bonding Active for C–H Bond Cleavage. *Inorg. Chem.* **2014**, *53*, 6634–6654. [CrossRef] [PubMed]
11. Oishi, M.; Kino, M.; Saso, M.; Oshima, M.; Suzuki, H. Early–Late Heterobimetallic Complexes with a Ta–Ir Multiple Bond: Bimetallic Oxidative Additions of C–H, N–H, and O–H Bonds. *Organometallics* **2012**, *31*, 4658–4661. [CrossRef]
12. Kameo, H.; Nakajima, Y.; Suzuki, H. Drastic Acceleration of Phosphine/Phosphite Incorporation into a Tetrahydrido Ruthenium/Osmium Complex, and One-way Ruthenium to Osmium Migration of a Phosphorus Ligand. *Angew. Chem. Int. Ed.* **2008**, *47*, 10159–10162. [CrossRef] [PubMed]
13. Alvarez, M.A.; García, M.E.; García-Vivó, D.; Huergo, E.; Ruiz, M.A. Synthesis of the Unsaturated $[MMoCp(\mu\text{-}PR_2)(CO)_5]^-$ Anions (M = Mn, R = Ph; M = Re, R = Cy): Versatile Precursors of Heterometallic Complexes. *Eur. J. Inorg. Chem.* **2017**, *9*, 1280–1283. [CrossRef]
14. Alvarez, M.A.; García, M.E.; García-Vivó, D.; Huergo, E.; Ruiz, M.A. Acetonitrile Adduct $[MoReCp(\mu\text{-}H)(\mu\text{-}PCy_2)(CO)_5(NCMe)]$: A Surrogate of an Unsaturated Heterometallic Hydride Complex. *Inorg. Chem.* **2018**, *57*, 912–915. [CrossRef] [PubMed]
15. Green, M.L.H.; Parkin, G. The Covalent Bond Classification Method and its Application to Compounds That Feature 3-Center 2-Electron Bonds. *Struct. Bond.* **2017**, *117*, 79–140.
16. García-Vivó, D.; Ruiz, M.A. Reply to the Comment on "Hydride, gold(I) and related derivatives of the unsaturated ditungsten anion $[W_2Cp_2(\mu\text{-}PCy_2)(\mu\text{-}CO)_2]$". *Dalton Trans.* **2018**, *47*, 6630–6631. [CrossRef] [PubMed]
17. Horton, A.D.; Mays, M.J.; Raithby, P.R. Synthesis and substitution reactions of a heterodimetallic molybdenum–manganese complex, $[MoMn(\mu\text{-}H)(\mu\text{-}PPh_2)(\eta^5\text{-}C_5H_5)(CO)_6]$; *X*-ray crystal structure of $[MoMn(\mu\text{-}H)(\mu\text{-}PPh_2)(\eta^5\text{-}C_5H_5)(CO)_4(\text{dppm-}PP')]$. *J. Chem. Soc. Dalton Trans.* **1987**, *6*, 1557–1563. [CrossRef]
18. Horton, A.D.; Mays, M.J.; Raithby, P.R. Formation of complexes with C···H···Mn interactions from reactions of dienes or acetylene with a μ-hydrido heterometallic dimer; *X*-ray crystal structures of $[(\eta^5\text{-}C_5H_5)MoMn(\mu\text{-}H)(\mu\text{-}PPh_2)(CO)_6]$, $[(\eta^5\text{-}C_5H_5)MoMn\{\mu\text{–}\sigma\text{:}\eta^3\text{-}CH_2C(Me)CHMe\}(\mu\text{-}PPh_2)(CO)_4]$, and $[(\eta^5\text{-}C_5H_5)MoMn\{\mu\text{–}\sigma\text{: }\eta^4\text{-}CHCHCH_2CHPPh_2\}(CO)_4]$. *J. Chem. Soc. Chem. Commun.* **1985**, *5*, 247–250. [CrossRef]
19. Cordero, B.; Gómez, V.; Platero-Prats, A.E.; Revés, M.; Echevarría, J.; Cremades, E.; Barragán, F.; Alvarez, S. Covalent Radii Revisited. *Dalton Trans.* **2008**, *21*, 2832–2838. [CrossRef] [PubMed]
20. Herberhold, M.; Wehrmann, F.; Neugebauer, D.; Huttner, G. Die photo-induzierte reaktion von dekacarbonyl-dimangan mit ammoniak, kristall- und molekülstrusktur des produkts $[fac\text{-}Mn(CO)_3(NH_3)_3][Mn(CO)_5]$. *J. Organomet. Chem.* **1978**, *152*, 329–336. [CrossRef]
21. Ni, C.; Lei, H.; Power, P.P. Reaction of M(II) Diaryls (M = Mn or Fe) with Ammonia to Afford Parent Amido Complexes. *Organometallics* **2010**, *29*, 1988–1991. [CrossRef]
22. Braterman, P.S. *Metal Carbonyl Spectra*; Academic Press: London, UK, 1975.
23. Carty, A.J.; MacLaughlin, S.A.; Nucciarone, D. *Phosphorus-31 NMR Spectroscopy in Stereochemical Analysis*; Verkade, J.G., Quin, L.D., Eds.; VCH: Deerfield Beach, FL, USA, 1987; Chapter 16.
24. Jameson, C.J. *Phosphorus-31 NMR Spectroscopy in Stereochemical Analysis*; Verkade, J.G., Quin, L.D., Eds.; VCH: Deerfield Beach, FL, USA, 1987; Chapter 6.
25. Cramer, C.J. *Essentials of Computational Chemistry*, 2nd ed.; Wiley: Chichester, UK, 2004.
26. Koch, W.; Holthausen, M.C. *A Chemist's Guide to Density Functional Theory*, 2nd ed.; Wiley-VCH: Weinheim, Germany, 2002.
27. Alvarez, M.A.; García, M.E.; García-Vivó, D.; Ruiz, M.A.; Toyos, A. The Doubly-Bonded Ditungsten Anion $[W_2Cp_2(\mu\text{-}PPh_2)(NO)_2]$: An Entry to the Chemistry of Unsaturated Nitrosyl Complexes. *Dalton Trans.* **2016**, *45*, 13300–13303. [CrossRef] [PubMed]
28. García, M.E.; Ramos, A.; Ruiz, M.A.; Lanfranchi, M.; Marchiò, L. Structure and Bonding in the Unsaturated Hydride- and Hydrocarbyl-Bridged Complexes $[Mo_2(\eta^5\text{-}C_5H_5)_2(\mu\text{-}X)(\mu\text{-}PCy_2)(CO)_2]$ (X = H, CH_3, CH_2Ph, Ph). Evidence for the presence of α-Agostic and π-Bonding Interactions. *Organometallics* **2007**, *26*, 6197–6212. [CrossRef]
29. Alvarez, M.A.; García, M.E.; García-Vivó, D.; Ruiz, M.A.; Vega, M.F. Synthesis and reactivity of the triply bonded binuclear anion $[W_2(\eta^5\text{-}C_5H_5)_2(\mu\text{-}PCy_2)(\mu\text{-}CO)_2]$: Tungsten makes a difference. *Organometallics* **2010**, *29*, 512–515. [CrossRef]

30. Alvarez, M.A.; García, M.E.; García-Vivó, D.; Ruiz, M.A.; Vega, M.F. Hydride, Gold(I) and Related Derivatives of the Unsaturated Ditungsten Anion $[W_2Cp_2(\mu\text{-}PCy_2)(\mu\text{-}CO)_2]$. *Dalton Trans.* **2014**, *43*, 16044–16055. [CrossRef] [PubMed]
31. Bader, R.F.W. *Atoms in Molecules—A Quantum Theory*; Oxford University Press: Oxford, UK, 1990.
32. Doyle, M.J.; Duckworth, T.J.; Manojlovic-Muir, L.; Mays, M.J.; Raithby, P.R.; Robertson, F.J. Substitution Reactions of a Heterodimetallic Molybdenum-Manganese Complex. *J. Chem. Soc. Dalton Trans.* **1982**, *18*, 2703–2714. [CrossRef]
33. Wrackmeyer, B.; Alt, H.G.; Maisel, H.E. Ein- und zwei-dimensionale Multikern NMR-Spektroskopie an den isomeren Halbsandwich-Komplexen *cis*- und *trans*-$[(\eta^5\text{-}C_5H_5)W(CO)_2(H)PMe_3]$. *J. Organomet. Chem.* **1990**, *399*, 125–130. [CrossRef]
34. Armarego, W.L.F.; Chai, C. *Purification of Laboratory Chemicals*, 7th ed.; Butterworth-Heinemann: Oxford, UK, 2012.
35. *CrysAlis Pro*; Oxford Diffraction Limited, Ltd.: Oxford, UK, 2006.
36. Farrugia, L.J. WinGX suite for small-molecule single-crystal crystallography. *J. Appl. Crystallogr.* **1999**, *32*, 837–838. [CrossRef]
37. Sheldrick, G.M. A short history of *SHELX*. *Acta Crystallogr. Sect. A* **2008**, *64*, 112–122. [CrossRef] [PubMed]
38. Sheldrick, G.M. Crystal structure refinement with *SHELXL*. *Acta Crystallogr. Sect. C* **2015**, *71*, 5–8. [CrossRef] [PubMed]
39. Frisch, M.J.; Trucks, G.W.; Schlegel, H.B.; Scuseria, G.E.; Robb, M.A.; Cheeseman, J.R.; Montgomery, J.A., Jr.; Vreven, T.; Kudin, K.N.; Burant, J.C.; et al. *Gaussian 03, Revision B.02*; Gaussian, Inc.: Wallingford, CT, USA, 2004.
40. Becke, A.D. Density-functional thermochemistry. III. The role of exact exchange. *J. Chem. Phys.* **1993**, *98*, 5648–5652. [CrossRef]
41. Lee, C.; Yang, W.; Parr, R.G. Development of the Colle-Salvetti correlation-energy formula into a functional of the electron density. *Phys. Rev. B* **1988**, *37*, 785–789. [CrossRef]
42. Grimme, S. Semiempirical GGA-type density functional constructed with a long-range dispersion correction. *J. Comput. Chem.* **2006**, *27*, 1787–1799. [CrossRef] [PubMed]
43. Hay, P.J.; Wadt, W.R. Ab initio effective core potentials for molecular calculations. Potentials for potassium to gold including the outermost core orbitals. *J. Chem. Phys.* **1985**, *82*, 299–310. [CrossRef]
44. Hariharan, P.C.; Pople, J.A. Influence of polarization functions on MO hydrogenation energies. *Theor. Chim. Acta* **1973**, *28*, 213–222. [CrossRef]
45. Petersson, G.A.; Al-Laham, M.A. A complete basis set model chemistry. II. Open-shell systems and the total energies of the first-row atoms. *J. Chem. Phys.* **1991**, *94*, 6081–6090. [CrossRef]
46. Petersson, G.A.; Bennett, A.; Tensfeldt, T.G.; Al-Laham, M.A.; Shirley, W.A.; Mantzaris, J. A complete basis set model chemistry. I. The total energies of closed-shell atoms and hydrides of the first-row elements. *J. Chem. Phys.* **1988**, *89*, 2193–2218. [CrossRef]
47. Portmann, S.; Luthi, H.P. MOLEKEL: An Interactive Molecular Graphics Tool. *CHIMIA* **2000**, *54*, 766–770.
48. Lu, T.; Chen, F. Multiwfn: A multifunctional wavefunction analyzer. *J. Comput. Chem.* **2012**, *33*, 580–592. [CrossRef] [PubMed]